Functional reorganization of visual processing following long-term adaptation to optical defects

Antoine Barbot[1,2], Woon-Ju Park[3,4], Ru-Yuan Zhang[3], Krystel R Huxlin[1,2,3], Duje Tadin[2,3], and Geunyoung Yoon[1,2#]

[1]Flaum Eye Institute, University of Rochester; [2]Center for Visual Science, University of Rochester; [3]Brain and Cognitive Sciences, University of Rochester; [4]Department of Psychology, University of Washington
[#]corresponding author: gyoon@ur.rochester.edu

Long-term exposure to poor ocular optics chronically alters the retinal input to the brain. Elucidating how this chronic change affects visual processing is vital for understanding the capacity for and limits of sensory plasticity in adults. Using adaptive optics to bypass the eye's optical defects, we assessed visual processing in neurotypically-developed adults with keratoconus—a corneal disease resulting in severe optical aberrations during adulthood. When tested under similar fully-corrected optical conditions as neurotypical observers, KC patients showed altered contrast sensitivity, with impaired sensitivity for fine spatial details and better sensitivity for coarse details. Both gains and losses in sensitivity were more pronounced in patients with poorer habitual optical quality, and were mediated by changes in signal enhancement mechanisms. The present findings uncover fundamental properties of neural compensation mechanisms in response to long-term exposure to optical defects, with a large-scale functional reorganization favoring sensory information less affected by the eye's optics.

Understanding how we see requires insights into the contribution of both optical and neural factors mediating visual perception, from the processing of images formed on the retina to the resulting perceptual representations. Visual processing is fundamentally limited by the eye's optics, which determine retinal image quality and constrain performance. Human optics, however, are not fixed and can substantially change over our lifespan and in disease[1]. Consequently, visual processing must be able to adapt to changes in sensory inputs over a range of different timescales and magnitudes. For instance, there is growing evidence that neural processing adapts to extended optical blur exposures, resulting in improved visual representations[2,3]. Neural adaptation mechanisms can compensate for blur-induced reductions in physical contrast of high spatial frequency (SF) retinal signals[3-6]. Even observers with typical optical quality show evidence of neural adaptation to their own optical blur, such that even modest changes in optical quality result in degraded subjective image quality[7].

Distinct neural adaptation mechanisms operate over different timescales[8-10]. Longer exposure to a given environment induces longer-lasting effects that are mediated by separate mechanisms from the ones controlling short-term adaptation[8,9]. Most studies investigated the effects of blur adaptation over relatively short-term periods (and often low magnitude of blur), thus limiting our understanding of how the adult human brain adapts to large changes in optical quality over long-term time periods (i.e., months to years). This, in turn, limits the development of clinical rehabilitations of a significant part of the population that experiences abnormal optics in their everyday life. A major experimental challenge comes from the difficulties of empirically isolating neural from optical factors. Technological advances in the field of adaptive optics (AO) offer a unique opportunity to bypass the limits imposed by optical factors while directly assessing visual processing of images free from any optical imperfections[11]. AO is a powerful technology that can be used to improve optical systems, including the human eye, by deforming a mirror to correct wavefront distortions of the optics (**Fig.1** and *Methods*). AO-correction in "healthy" eyes allows observers to detect a larger range of high-SF information, otherwise indiscernible

in the presence of typical optical blur, improving visual acuity[12] and contrast sensitivity[13]. More importantly, AO correction can be used to assess how changes in optical quality alter neural functions by making it possible to compare visual processing under fully-corrected optical quality of both typical "healthy" eyes[7,12-14] and those with severe optical abnormalities[15-17].

In this context, keratoconus (KC) represents an ideal model of long-term neural adaptation to optical defects. KC is a severe corneal disease afflicting young to middle-aged, neurotypically-developed adults (**Fig.1a**). In this condition, the corneal stroma progressively thins and assumes a conical shape, resulting in a substantial increase both in lower-order (defocus and astigmatism) and higher-order (HOAs) aberrations. Although HOAs are relatively small in typical eyes, abnormal corneal conditions (e.g., such as KC) can cause large magnitudes of HOAs that cannot be efficiently corrected by conventional optical devices[18,19]. Thus, despite their habitual optical correction, KC patients are constantly exposed to substantially degraded retinal inputs in their everyday life, which limits visual function. The prolonged exposure to poor optical quality results in neural adaptation that alters visual processing and limits the benefits of improved optical correction. When tested under full AO-correction, KC patients exhibit considerably poorer visual acuity[16] than that predicted by optical theory or measured in neurotypical observers with similar AO-corrected optical quality. However, little is known regarding the underlying mechanisms mediating such changes in visual processing following long-term adaptation to severe optical aberrations.

Here, we used state-of-art AO to assess how long-term exposure (i.e., years) to optical defects alters neural processing of visual information in neurotypically-developed humans. To do so, we measured the impact of different amounts of optical aberrations experienced by neurotypical (NT) observers and KC patients on the visual system's ability to detect contrast over a wide range of SFs, which is the foundation for the brain's coding of visual information. The visual system is composed of SF-selective filters whose combined sensitivity determines the shape of the contrast sensitivity function (CSF)[20-22]. For well over a century, contrast sensitivity has been a valuable tool for measuring the limits of visual perception, as well as for the assessment and early diagnosis of many disorders[21,23]. The detection of changes in the shape of the CSF can allow inferences about changes in underlying physiological processes, such as in amblyopia[24], autism spectrum disorder[25], and aging[26]. As the impact of optical aberrations in KC patients is more pronounced for high SFs, we expect deficits in contrast sensitivity at high SFs despite correcting all optical aberrations with AO, whereas sensitivity to low-SF information should remain unaffected. However, whether neural processing in KC is simply impaired for visual inputs affected by the eye's optics or undergoes a more adaptive functional reorganization is unknown. In two experiments, we provide compelling evidence of neural compensation for severely degraded retinal inputs experienced over prolonged periods of time. First, we show altered CSF and poorer visual acuity in KC patients relative to age-matched NT observers, despite being tested under AO correction. Then, using an equivalent noise paradigm and a computational model of visual processing[27-33], we uncover the putative mechanisms underlying changes in visual sensitivity observed in KC patients under AO correction. Overall, our findings reveal that chronic exposure to poor optical quality does not result in neural deficits restricted to high SFs, but rather manifests by large-scale changes in visual sensitivity across a broad range of SFs via changes in signal enhancement mechanisms.

Results

Habitual aberrations and AO-corrected visual quality. We first needed to quantify the amount of habitual optical aberrations experienced by each observer, before establishing that we can fully correct all optical aberrations to a similar level in both neurotypical (NT) observers and KC patients with varying levels of optical defects. Habitual optical quality was estimated using the AO visual system (AOVS; **Fig.1b** and **Fig.S1**) by collecting multiple wavefront measurements for each observer wearing their own, everyday optical corrective method, if any. The wavefront maps were fitted with Zernike polynomials to compute the total RMS and higher-order RMS (hRMS+; HOAs only) for a 6-mm pupil (**Fig.1c**; see also *Methods* and **Table S1**). Relative to optical quality in age-matched NT observers (total RMS: 0.91±0.31 µm; range: 0.57-1.44 µm), habitual optical quality in KC eyes (total RMS: 3.19±2.2 µm; range: 1.35-7.84 µm), remained sub-optimal despite their own optical corrections (*typical vs KC total RMS*: Welch's t-test, t=3.08, *p=0.014*, d=1.45). Specifically, KC eyes were subject to a substantial amount of uncorrected HOAs (hRMS+: 1.90±1.35 µm; range: 0.33-4.55 µm), much more than in NT eyes (hRMS: 0.35±0.11 µm; range: 0.22-0.55 µm) (*NT vs KC hRMS+*: Welch's t-test, t=3.43, *p=0.009*, d=1.62). As previously reported[19], KC eyes were particularly affected by large amounts of vertical coma (mean absolute Z_7 coefficient: 1.38±1.02 µm, range: 0.03-2.88), much more than in typical eyes (mean absolute Z_7 coefficient: 0.13±0.12 µm, range: 0.02-0.34).

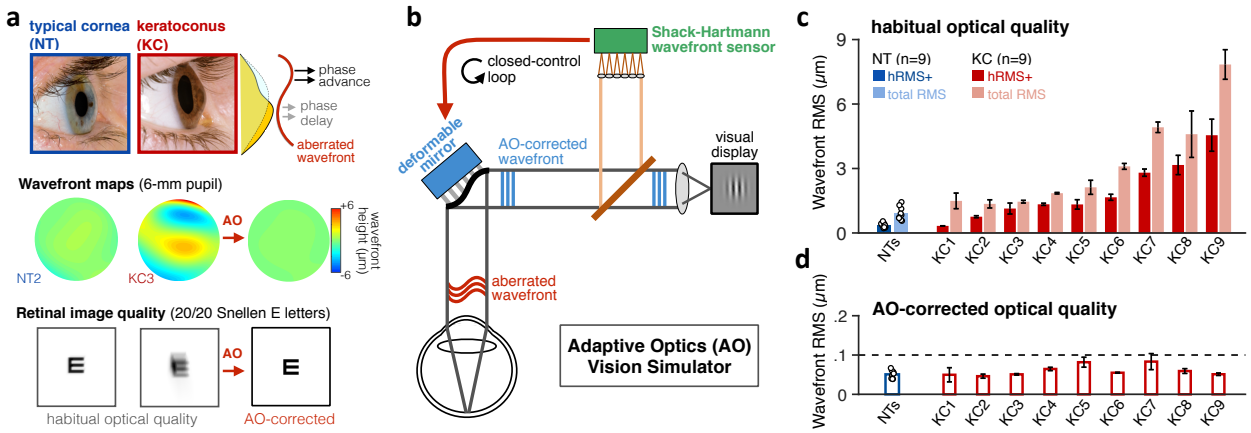

Figure 1. *Using adaptive optics to study long-term neural adaptation to poor optics in keratoconus.* **(a)** KC is a progressive eye disease affecting neurotipically-developed young adults, in which the normally round cornea thins and begins to bulge into a cone-like shape. KC results in large amounts of higher-order optical aberrations (HOAs), as shown on the wavefront maps, which cannot be fully corrected and degrade retinal image quality. Adaptive optics (AO) allows to fully correct optical quality and assess the impact of long-term exposure to severe optical aberrations on visual processing. **(b)** Our AO vision simulator can maintain aberration-free image quality during visual testing, by measuring the aberrated wavefront of the participant's eye using a Shack-Hartmann wavefront sensor and fully correcting it online with a deformable mirror in closed-control loop. **(c)** Relative to neurotypical (NT) eyes, KC eyes were exposed to severe optical defects in their everyday life, particularly large amounts of HOAs (hRMS+). Group-average total RMS and hRMS+ for NTs are represented with each data point corresponding to an individual subject. Individual bars show the habitual RMS for each KC separately, with error bars corresponding to ±1 SD. **(d)** AO correction allowed us to bypass optical defects and maintain aberration-free optical quality (i.e., residual total RMS ~0.05 µm), even in severe KC eyes. Note the large difference in y-axis scale between panels c and d.

Consistent with previous studies from our lab[15-17,34], our AO system allowed us to measure visual performance while effectively maintaining aberration-free optical quality, even in severe KC eyes (**Fig.1c** and **Fig.S2**). Full AO-correction was applied during all testing sessions. To maximize AO correction during stimulus presentation, observers were trained to blinks between trials and to pause if the perceptual quality got unstable or poor quality during testing. Continuous closed-loop AO correction during visual testing resulted in a residual wavefront RMS that remained not significantly different from 0.055 µm for both NT eyes (residual RMS: 0.051±.01 µm; Student t-test: t(8)=1.24, *p=.251, d=0.41*) and KC eyes (residual RMS: 0.060±.014 µm; Student t-test: t=1.13, *p=.292, d=.38*). More important, aberration-free optical quality under AO correction was similar between NT and KC eyes (Student t-test, t=1.64, *p=0.120*, d=0.77), with no relation between AO performance and the severity of the habitual RMS (Pearson's correlation: total RMS r=+.32, *p=.196;* hRMS+ r=+.35, *p=.157*). Thus, online AO correction effectively and continuously corrected all optical aberrations during visual testing, allowing us to bypass optical factors and assess differences in neural processing between NT and KC observers under similar aberration-free conditions.

Altered contrast sensitivity function following long-term adaptation to optical defects. In Experiment 1, we assessed the CSF in both KC (N=9) and age-matched NT (N=9) observers under aberration-free conditions. The CSF characterizes visual sensitivity to gratings of different SFs (in cycle per degree or cpd), where sensitivity is defined as the reciprocal of the contrast threshold. Observers performed an orientation discrimination task at fixation (**Fig.2a**) in which they reported the orientation of ±45º-tilted Gabor patches varying in SF and contrast. To optimize data collection, we used the *quick CSF* method[24,35], which combines Bayesian adaptive inference with a trial-by-trial information gain strategy to estimate the observer's CSF as a truncated log-parabola with four parameters (**Fig. 2b** and *Methods*): (1) the peak sensitivity $CS_{\max}$; (2) the peak frequency SF_{peak}; (3) the bandwidth β; and (4) the truncation level at low SF δ. The low-SF truncation level determines the sensitivity at low SF (CS_{low}). We also estimated the high-SF cutoff (SF_{cutoff}) from the qCSF fits—a measure of visual acuity. The qCSF method has been used to characterize CSF in both neurotypical and in diverse clinical populations[24,35-39].

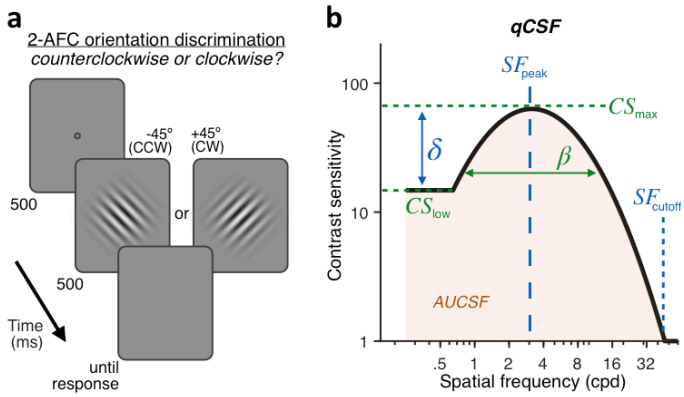

Figure 2. Experiment 1: Contrast Sensitivity Function (CSF) measurement. **(a)** *Stimuli task, and timeline.* Each trial began with a dynamic fixation point (see *Methods*). After a blank screen, a Gabor stimulus was presented at fixation using a temporal Gaussian envelope. Stimuli were ±45º oriented Gabors varying in contrast and spatial frequency (SF) from trial to trial. Observers judged whether the stimulus was tilted left or right from vertical. Full AO correction was maintained during the testing. **(b)** *The quick CSF method.* The qCSF method efficiently estimates the CSF through 4 parameters: peak sensitivity ($CS_{\max}$), peak SF (SF_{peak}), bandwidth (β), and low-SF truncation (δ). The area under the CSF (AUCSF), low-SF sensitivity (CS_{low}), and high-SF cutoff (SF_{cutoff}) were also estimated from the qCSF fits.

Under similar, aberration-free optical quality, KC participants exhibited altered CSF relative to NT observers, showing both impairments for high SFs (*p<0.05* for SF≥5.3 cpd) as well as improvements for low SFs (*p<0.05* for SF≤0.6 cpd) (**Fig.3a**). In other words, even when both groups had matched retinal image quality, there were still substantial differences in visual sensitivity. This pattern of gains and losses changed the shape of the CSF, revealing both impaired sensitivity at high SFs (SF_{cutoff}; NT: 41.3 cpd [39.2–44.7; 95%-CI]; KC: 32.2 cpd [30.8–35.3; 95%-CI]; *p<0.001*) and better sensitivity at low SF (CS_{low}; NT: 4.92 [4.03–6.46]; KC: 8.64 [6.72–10.22]; *p=0.0012*). Improved low-SF sensitivity reflected a reduced low-SF truncation level in KC (δ; NT: 1.23 [1.13–1.32]; KC: 0.94 [0.87–1.06]; *p<0.001*). Notably, the impairment in high-SF cutoff correlated with the reduction in low-SF truncation across observers (r= .47, *p=0.047*)—a pattern of results that is suggestive of a functional reorganization of visual processing across SFs. The overall result was a shift in peak SF towards lower SFs in KC patients relative to NT observers (SF_{peak}; NT: 3.42 cpd [3.25–3.83]; KC: 2.84 cpd [2.67–3.11]; *p<0.001*). Notably, no significant changes in amplitude (CS_{max}; NT: 82.6 [76.2–94.2]; KC: 75.8 [66.8–88.5]; *p=0.128*) or bandwidth (β; NT: 2.83 [2.64–2.98]; KC: 2.77 [2.60–2.92]; *p=0.338*) were observed. These changes resulted in the area under the CSF (AUCSF) to be slightly reduced in KC participants (AUCSF; NT: 2.81 [2.77–2.90]; KC: 2.73 [2.66–2.81]; *p=0.025)*. Note that AUCSF depends on the SF range used to define the area. Had we used additional low SFs in our experiment, where KC patients showed improved performance, the difference in AUCSF between groups would have been attenuated, and perhaps eliminated.

Critically, both gains and losses in CSF under aberration-free conditions were more pronounced in severe KC, who experienced large amounts of habitual aberrations in their everyday life (**Fig.3b** and **Fig.S3**). Changes in qCSF parameters under full AO correction correlated with the amount of habitual aberrations observers experienced in their everyday life (**Fig.3c**; Pearson's correlation coefficients using habitual total RMS; SF_{peak}: r=-.71, *p<0.001*; SF_{cutoff}: r=-.79, *p<0.001*; δ: r=-.80, *p<0.001;* CS_{low}: r=+.62, *p=0.006*). No correlation was observed between habitual optical quality and other qCSF parameters (CS_{max}, β, or AUCSF). A similar pattern was observed using hRMS+ as an index of habitual optical quality (**Fig.3c**). Furthermore, visual acuity (VA) measurements using high-contrast Snellen E letters (see *Methods* and **Fig.S4**) showed poorer acuity in KC patients (15.14±1.64, range: 13.38-17.81) than predicted from optical theory or NT observers (11.97±0.94, range: 10.58-13.61), despite being tested under full AO correction (*NT vs KC VA in logMAR*: Student t-test, t=5.34, *p<0.001*, d=2.52). This deficit in high-contrast VA is consistent with previous findings[16] and correlated with the amount of habitual aberrations experienced by each observer (total RMS: r=+.85, *p<.001*; hRMS+: r=+.87*, p<.001*), as well as with the changes in peak SF (SF_{peak}; r=-.74, *p<.001*), high-SF cutoff (SF_{cutoff}; r=-.77, *p<.001*), and notably low-SF truncation (δ; r=-.72, *p<.001*) and low-SF sensitivity (CS_{low}; r=+.61, *p=.007*). That is, poorer visual acuity in KC under AO correction is predicted by both impaired sensitivity at high SFs as well as enhanced sensitivity to low SFs. These results indicate that long-term exposure to severe optical aberrations alters the CSF in a way that results in impaired fine spatial vision but also in better sensitivity to coarser spatial information less affected by optical aberrations. The resulting large-scale change in contrast sensitivity across SFs is expected to optimize neural sensitivity to severely aberrated retinal images caused by KC, but limits neural processing of fine spatial details under aberration-free optical quality.

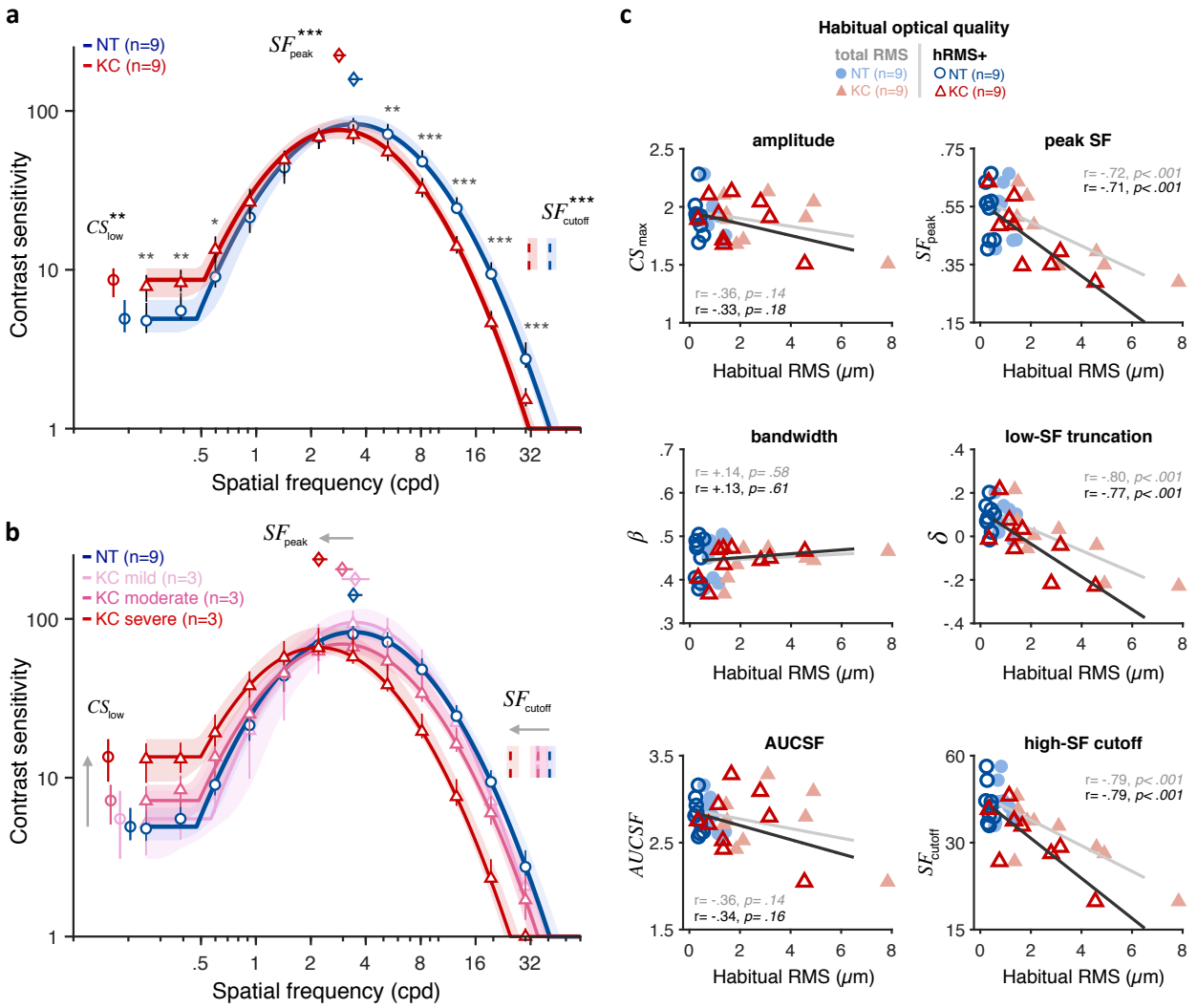

Figure 3. Experiment 1: *Altered contrast sensitivity function (CSF) following long-term neural adaptation to poor optics.* All results are for AO-corrected visual images for both keratoconus (KC) and neurotypical (NT) observers. **(a)** *qCSF results*. Relative to NT observers (blue curve), KC patients (red curve) showed altered CSF that were shifted towards lower SFs, with impaired high-SF sensitivity and improved low-SF sensitivity. Shaded areas and error bars represent bootstrapped 95%-CI. Asterisks indicate significant differences computed from bootstrapping between NT and KC groups (*: *p<0.05*; **: *p<0.01*; ***: *p<0.001*). **(b)** Same as (a) with KC patients divided into 3 equal groups based on KC severity (see also Fig.S3). **(c)** *Link between CSF and habitual RMS*. Altered CSF under AO correction correlated with the amount of habitual aberrations of each subject. Each panel shows individual parameter estimates plotted as a function of each subject's habitual RMS (total RMS: darker open symbols; hRMS+: light filled symbols). Linear regression fits and correlation coefficients are plotted for each RMS condition.

Altered internal noise properties following long-term adaptation to optical defects. To better understand how long-term exposure to optical defects alters visual processing across SFs, we used an equivalent noise paradigm[27-33] where perceptual thresholds are measured as a function of varying external noise levels added to the stimuli (see *Methods*). Six participants from each group (**Table S1**) performed an orientation discrimination task under varying levels of dynamic white noise (**Fig.4a**), judging whether a foveally-presented grating was tilted ±45° from the vertical. Stimulus presentation was controlled using the *FAST* method[40], an advanced adaptive psychophysical technique which allowed us to estimate relevant model parameters in just 480 trials per participant[27-33]. Changes in thresholds

with external noise levels result in a characteristic threshold-versus-noise (TvN) function, which can be fitted with the Perceptual Template Model (PTM)[27-29] to quantify the effects of noise on perception (**Fig.4**). The PTM is a computational vision model of visual processing that had been successfully used to identify the mechanisms underlying perceptual differences for a wide range of brain functions (e.g., attention[41-43], perceptual learning[27,28]) and between specific populations (e.g., amblyopia[44], autism[32], dislexya[45], cortical blindness[46]). The PTM considers that differences in perceptual performance between groups can result from changes in three possible sources of noise (**Fig. 4b**): (1) internal additive noise (A_{add}); (2) external noise filtering (A_{ext}); and (3) internal multiplicative noise (A_{mul}). Increased internal additive noise leads to worse perceptual thresholds at low external noise levels, reflecting impaired signal enhancement of the perceptual template (**Fig. 4c**, *upper left*). Poorer external noise filtering impairs performance at higher external noise levels, reflecting poorer signal selectivity (tuning) of the perceptual template (**Fig. 4c**, *upper right*). A combined effect of higher internal additive noise and poorer external noise filtering would elevate thresholds at all external noise levels, similarly across difficulty levels (**Fig. 4c**, *lower left*). In contrast, higher internal multiplicative noise (A_{mul}) would also impair thresholds across external noise levels, but via a non-uniform shift in the TvN functions across difficulty levels (**Fig. 4c**, *lower right*). Higher A_{mul} results in stronger elevation in internal noise with signal contrast, acting similarly to a contrast gain control mechanism (i.e., compressive response at higher contrasts).

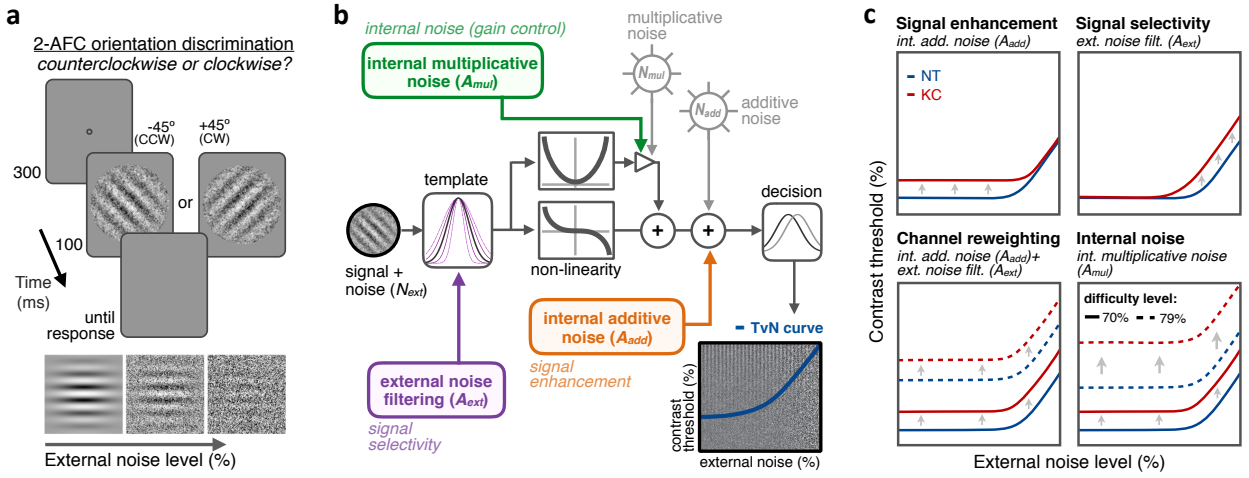

Figure 4. Experiment 2: *SF-specific changes in visual processing following long-term adaptation to poor optics.* All results are for AO-corrected visual images for both KC and NT. **(a)** *Stimuli, task, and timeline.* Each trial began with a dynamic fixation point. After a blank screen, an oriented grating embedded in dynamic Gaussian pixel noise was presented. Observers judged whether the grating was tilted ±45° from vertical. **(b)** *Schematic representation of the Perceptual Template Model (PTM).* The PTM consists of five main components: a perceptual template processing the signal embedded in external noise (N_{ext}), a nonlinear transducer function, two internal noise sources (multiplicative N_{mul} and additive N_{add}), and a decision process. The output of the decision process models limitations in sensitivity as equivalent internal noise, with threshold-vs-noise (TvN) curves having a characteristic nonlinear shape. At low external noise, internal noise dominates and added external noise has little effect, resulting in the TvN curve's flat segment. Once external noise level exceeds that of internal noise, stronger signal contrast is needed to overcome added external noise, resulting in the TvN curve's rising segment. Adapted from[29]. **(c)** *Predictions.* The PTM evaluates distinct mechanisms that can account for differences between NT and KC observers. (1-*upper left*) Elevated internal additive noise (A_{add}) yields in increased thresholds at the flat portion of the curve, reflecting signal enhancement changes; (2-*upper right*) Poorer external noise filtering (A_{ext}) limits thresholds at the rising portion of the curve, reflecting signal selectivity changes. (3-*lower left*) A combination of the two will result in increased thresholds across external noise levels and across difficulty levels, reflecting channel reweighting; (4-*lower right*) Elevated internal multiplicative noise (A_{mul}) would result in a similar pattern across external levels but the differences would scale with difficulty levels.

First, we analyzed the data using the conventional PTM[27-29] (see *Methods*) to characterize the relative difference in noise-limiting factors between groups and across SFs. To do so, contrast thresholds were estimated for each observer, at each external noise level, SF, and difficulty level (**Fig.5**). These independent threshold estimates were noisy, given that our empirical approach was optimized for estimating relevant model parameters with a limited number of individual trials. To characterize the impact of habitual optical quality on contrast thresholds as a function of SF, external noise and difficulty levels, we fitted the PTM to the data in a conventional manner using a least-squares procedure[27-29]. Given the large individual variability in KC habitual aberrations and its impact on the CSF, KC participants were split into 2 groups based on KC severity using a median split (total RMS: 3.85 µm; hRMS+: 2.23 µm), resulting in three groups based on habitual optical quality (**Table S1**): neurotypical (N=6; total RMS: 0.91±0.33 µm; hRMS+: 0.35±0.12 µm), mild/moderate KC (N=3; total RMS: 2.19±0.87 µm; hRMS+: 1.25±0.46 µm), and severe KC (N=3; total RMS: 5.78±1.79 µm; hRMS+: 3.51±0.92 µm). The data from all SFs were included in the analysis, with the model estimating separate TvNs for each group, each SF, and each difficulty levels. The resulting TvN curves estimated by the PTM exhibited characteristic nonlinear patterns (**Fig.5**).

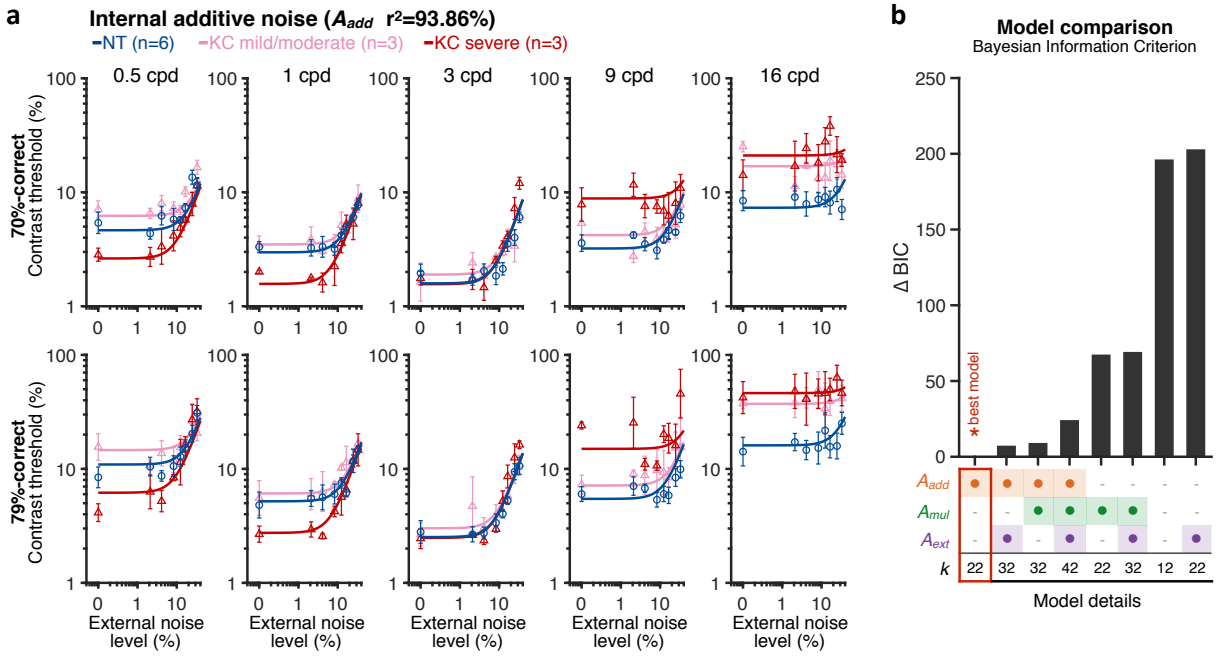

Figure 5. *Changes in internal additive noise mediate contrast sensitivity differences in KC across SFs.* **(a)** Contrast threshold estimates were measured under AO correction for Gabor stimuli embedded in different levels of external white noise, for five different spatial frequencies (0.5, 1, 3, 9, and 16 cpd) and at either 70.71%-correct (*upper row*) and 79.37%-correct (*lower row*) difficulty levels. Relative to NT observers, participants with severe KC showed better contrast thresholds at low SFs, and impaired thresholds at high SFs. These differences under aberration-free optical conditions were observed at low, but not at high external noise levels, and were less pronounced in observers with mild-to-moderate amounts of habitual optical aberrations. Data were fitted with the PTM to evaluate the contribution of distinct sources of inefficiencies: internal additive noise (A_{add}), internal multiplicative noise (A_{mul}), external noise filtering (A_{ext}), or any combination of these factors. The best model explaining the differences between NT and KC groups was the internal additive noise model (r^2=93.9%; see *Supplementary Information*). **(b)** *Model comparisons*. Bayesian Information Criterion (BIC) evidence was computed for each model to identify which model best explains the data while taking into account the number of free parameters (*k*) of each model. The value of the best model was subtracted from all BIC values (ΔBIC), with the best model (ΔBIC = 0) being a model assuming solely changes in internal additive noise across SFs between NT and KC groups.

To assess mechanisms underlying differences in contrast sensitivity between groups, several variants of the PTM were fit to the data (**Fig. 5a**; see also **Table S2** and **Fig.S5-8**): no group difference (null model), changes in internal additive noise (A_{add}), external noise filtering (A_{ext}), or internal multiplicative noise (A_{mul}), mixtures of them (A_{add}+A_{mul}; A_{add}+A_{ext}; A_{mul}+A_{ext}), and a full model assuming changes in all three mechanisms (A_{add}+A_{ext}+A_{mul}). To account for the differences in the number of free parameters across models, we computed the Bayesian Information criterion (BIC) to assess which model best fits the data while penalizing for greater number of free parameters. Overall, we found that the differences in contrast thresholds between NT and KC groups were best explained by a simple model assuming solely SF-dependent changes in internal additive noise (r^2=93.9; **Fig. 5a** and **Table S3**), without changes in external noise filtering and/or internal multiplicative noise. Relative to NT participants, severe KC participants showed a reduction in internal additive noise (A_{add}) by -42.6% and -46.3% at 0.5 and 1 cpd, respectively. Mild/moderate KC patients did not show such benefits at low SFs, but rather an elevation in internal noise by +32.8% and +16.8% at 0.5 and 1 cpd, respectively. At 3 cpd, mild/moderate KC observers were slightly worse than NT observers due to elevated internal additive noise (+18.9%), whereas severe KC patients showed a negligible reduction in internal noise (-1.6%). At high SFs, all KC participants exhibited impaired contrast thresholds due to large elevations in internal additive noise, by +30.1% and +126.4% at 9 and 16 cpd for mild/moderate KCs, and by +167.7% and +179.7% at 9 and 16 cpd, for severe KC patients. Additional PTM analyses, separately for low and high SFs, further supported SF-specific changes in internal additive noise as the primary mechanism underlying altered CSF following long-term exposure to poor optical quality (see *Supplementary Information* and **Fig.S9-10**). The pattern of gains and losses in sensitivity across SFs at low external noise levels is consistent with the alterations of the CSF observed in Experiment 1 (**Fig.S11**).

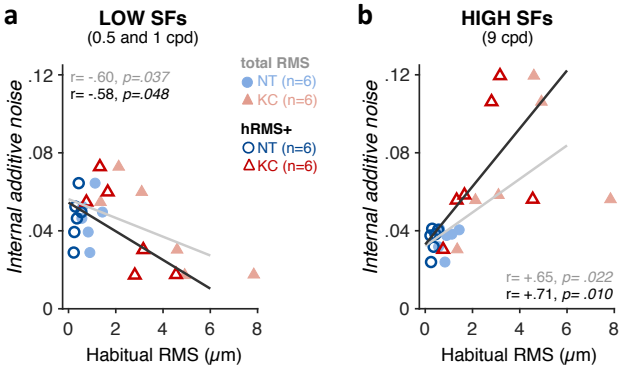

Figure 6. *Correlation between individual internal additive noise estimates and participants' habitual optical quality.* **(a)** Poorer habitual optical quality was associated with reduced internal additive noise at low SFs (i.e., improved signal enhancement). For each observer, we averaged individual internal additive noise estimates at 0.5 and 1 cpd. **(b)** At high SFs (9 cpd), the opposite pattern was found, with poorer habitual optical quality being associated with elevated internal additive noise. Consistent with internal additive noise being the primary source of inefficiency mediating the effects of long-term exposure to poor optical quality, other noise estimates (i.e., internal multiplicative noise and external noise filtering) did not correlate with participants' habitual optical quality (see Fig.S12).

To better assess individual differences in underlying sources of altered perception across SFs and relate them to each observer's habitual optical quality, we used a hierarchical Bayesian model to estimate TvN curves and parameter estimates for individual participants (see *Methods*). By assuming that the variability between participants follows a population-level distribution, this analysis allowed us to reduce some of the noise in individual parameter estimates. We then tested whether the level of internal additive noise, as well as other PTM estimates, correlated with the amount of each participant's habitual RMS. Consistent with the SF-specific changes in sensitivity observed in KC patients, poorer

habitual RMS was associated with reduced individual internal additive noise levels at low SFs (0.5 and 1 cpd) (**Fig.6a**; total RMS, r=-.60, *p=0.037*; hRMS+, r=-.58, *p=0.048*). At high SFs, individual noise estimates were more variable, particularly at 16 cpd where we could not reliably estimate the non-linear segment of individual TvN curves. As a result, we restricted our analysis to individual noise estimates from the 9 cpd condition. We found that poorer habitual optical quality was positively correlated with elevated individual internal additive noise levels at high SFs (**Fig.6b**; total RMS, r=+.65, *p=0.022*; hRMS+, r=+.71, *p=0.010*). No correlation was found with either internal multiplicative noise (A_{mul}) or external noise filtering (A_{ext}) for low or high SFs (**Fig.S12**), supporting the fact that the effects of long-term exposure to various magnitudes of habitual optical aberrations are best explained by an internal additive noise model that assumes SF-specific changes in signal enhancement.

Taken together, the present findings show that long-term exposure to poor optical defects causes a large-scale functional reorganization in visual sensitivity across SFs, which reflects SF-specific changes in signal enhancement mechanisms of SF-selective neurons. The atypical contrast sensitivity and poorer acuity observed in neurotypically-developed adults with severe optical defects, even when all optical aberrations are bypassed using AO correction, reflect long-term neural compensation mechanisms that improve visual processing of the degraded retinal inputs but limit the clinical benefits of improved optical correction in these patients.

Discussion

The present study combined advanced optics, psychophysical and computational methods to assess neural adaptation in response to long-term (i.e., up to 20 years) exposure to poor optical quality. An AO vision simulator was used to fully bypass optical limitations and directly access and isolate visual function in human adults, who are otherwise exposed to various amounts of optical aberrations. Our results provide evidence of large-scale functional reorganization of sensory resources following long-term exposure to severely degraded retinal inputs. Under fully-corrected optical conditions, KC patients showed a loss in sensitivity to high-SF information, which was due to poorer signal enhancement mechanisms of high-SF selective filters. Moreover, severe KC patients showed enhanced sensitivity to low-SF information, which reflected improved signal enhancement mechanisms of low-SF selective filters. Notably, magnitudes of observed enhancements at low SFs and impairments at high SFs were correlated across observers, and both effects were more pronounced in more severe KC cases. This pattern of gains and losses in visual sensitivity reveals fundamental properties of adaptive neural mechanisms compensating for the chronic exposure to blurred retinal images.

A key function of sensory systems is to adapt to our sensory environment. Contrast sensitivity is the foundation for the brain's coding of visual information and is central for characterizing both visual function and clinical disorders. The shape of the CSF likely reflects the visual system's sensitivity to stimulus properties that are useful for perception. In neurotypical observers, the drop in sensitivity at high SFs is mostly due to blurring from the eye's optics[21,47]. Optical blur reduces the strength and reliability of high-SF retinal inputs, leading to weak and unreliable neural responses to fine spatial details. In KC, optical aberrations become ~6 times worse compared to typical levels[19], strongly attenuating high-SF retinal signals and depriving the visual system from fine spatial information. Our

findings show that the severe and prolonged exposure to optically degraded retinal inputs under natural viewing results in neural insensitivity to fine spatial details, even when viewing images that are near-perfect optically. Using the PTM, we demonstrated that this neural insensitivity to high-SF signals was due to elevated levels of internal additive noise (i.e., reduced signal enhancement) of high-SF filters. Internal noise impairs the reliability of sensory representations, and is a key factor in perceptual variability within the nervous system[48]. This increase in internal noise levels of high-SF selective filters can account for the fact that when tested under AO correction, KC patients show considerably poorer high-contrast letter acuity than observers with typical optical quality whose AO-corrected acuity approaches the limit imposed by photoreceptor sampling[16,17].

More important, chronic exposure to degraded high-SF inputs did not solely induce impairments in high-SF visual function. Participants with severe KC also showed better contrast sensitivity to low-SF signals under AO correction, paired with reduced levels of internal additive noise. Thus, the effects of long-term exposure to poor ocular optics cannot be simply characterized as deficits at high SFs, but rather as altered visual sensitivity across SFs via changes in signal enhancement mechanisms that attenuate high-SF signals while enhancing low-SF information. This pattern of gains and losses in sensitivity can be understood by considering how habitual optics of KC eyes affect retinal image quality. While optical blur strongly degrades high-SF signals, lower SFs are less compromised by blur and become predominant and more reliable than higher SFs, especially under large amounts of blur. As a result, KC patients are in a low-pass state of adaptation during natural vision, relying more on low-SF information to interact with their environment. Following short-term blur adaptation, humans with typical optical quality usually show enhanced sensitivity for high SFs and reduced sensitivity for low SFs[49,50]. In contrast, our results show that blur adaptation over considerably longer periods of time has opposite effects on contrast sensitivity, supporting the notion that distinct neural adaptation mechanisms operate over different timescales[8-10].

Adaptation acts to maintain sensory systems operating within the limited dynamic range afforded by the brain's limited resources[51], serving as optimal resource allocation that can manifest in large-scale reorganization in neural sensitivity[52]. In this context, the CSF reflects an optimal allocation of the brain's limited sensory resources to process a wide range of spatial details. The pattern of gains and losses in sensitivity we observed could reflect neural compensation mechanisms that optimize visual processing to the structure of the degraded retinal inputs. For instance, short-term adaptation to different stimulus speeds results in a large-scale reorganization of the spatiotemporal CSF, which optimizes neural sensitivity to the new environment[52]. Physiologically, cells in the primary visual cortex (V1) adaptively change their responses to match the input properties of natural (broadband) stimulation and enhance information transmission in visual processing[53]. Moreover, brief adaptation to even a single stimulus can reorganize neuronal correlations across an entire network, resulting in specific, stimulus-dependent changes in the population code's efficiency[54]. What is unknown, however, is what kinds of neural changes occur during years long adaptation periods, as experienced by patients with severe optical defects such as KC patients. We conjecture that such long-term exposure to severely degraded retinal image quality results in a reallocation of the brain's limited sensory resources, improving visual processing in KC patients across many stimuli and tasks. Indeed, while KC participants suffer from poorer visual acuity under full AO-correction, they actually show better acuity (i.e., by +24%) under their own

optical quality than typical observers tested under the same degraded optical conditions[55]. Moreover, contrast adaptation

Our methods are largely agnostic about the neural bases of long-term adaptation to poor optical quality. We hypothesize that our findings are likely to be due, at least partially, to neural changes occurring in V1. Pooled responses of V1 neurons can predict behavioral performance in contrast sensitivity tasks[56], and the perceptual CSF and neuronal CSF in V1 are highly correlated[57,58], sharing a similar shape, peak SF and amplitude. That is, the shape of the perceptual CSF is assumed to reflect properties of V1 neurons selective to a wide SF range. While responses in the lateral geniculate nucleus (LGN) are primarily low-pass in SF, the majority of V1 neurons possess bandpass characteristics. The fall-off of the CSF at low SFs is generally attributed to lateral inhibition in retinal ganglion cells[59], as well as normalization–a canonical neural computation in which the response of an individual neuron is divided by the summed activity of a pool (population) of neurons[60]. As retinal mechanisms tend to be less plastic, long-term adaptation effects on visual sensitivity observed in KC patients could reflect changes in normalization in V1. Divisive normalization plays an important role in determining visual sensitivity, serving as a form of homeostatic control of V1 functional properties that optimize the network nonlinearities to the statistical structure of the visual input[61]. Here, severe optical blurring in KC eyes would reduce the contribution of high-SF neurons to the normalization pool, in turn increasing the response of neurons selective to lower SFs. Another, not mutually exclusive, neural account could involve interactions between SF-selective channels[50,62-64]. For instance, SF-specific inhibitory mechanisms have been shown to refine SF selectivity of V1 neurons[62]. SF-specific inhibition of low SFs plays a key role in the generation of bandpass V1 selectivity[63,64], shifting the preferred spatial selectivity to higher SFs. Moreover, adaptation effects at different spatial scales are not independent[50], ruling out simple linear filter models of cortical processing. Changes in normalization and/or SF-specific inhibition mechanisms would involve large-scale changes in neural sensitivity across many V1 neurons selective to a wide range of SFs, consistent with the SF-specific changes in sensitivity we observed in KC patients. Note that we cannot unequivocally rule out other types of plasticity that could affect the shape of the CSF, such as changes in the number of neurons selective for different SFs[20].

The effects of prolonged exposure to poor optical quality may also be interpreted as a form of perceptual learning. Under natural viewing, KC patients who are continuously exposed to severely degraded images have to relearn how to interact with their environment, which is extremely rich in terms of tasks and stimulus properties. Visual adaptation[2,3,65] and perceptual learning[66,67] are two forms of experience-dependent plasticity that can interact, despite having distinct neural mechanisms and perceptual consequences. For instance, perceptual learning has been shown to reconfigure the effects of visual adaptation[68]. Indeed, while adaptation reduces sensitivity prior to training, learning while in an adapted state can reverse the effects of adaptation, leading to an overall benefit after training[68]. This reversal in adaptation effects following repetitive training was specific to the trained, adapted state, while untrained, adapted states were associated with significant costs in sensitivity following training[68]. Such interactions between sensory adaptation and perceptual learning mechanisms may also account for some of the differences in adaptation effects over brief and long-term timescales[8-10]. Long-term adaptation to severe optical aberrations induces long-lasting effects on visual processing that limit the clinical benefits of improved optical correction. Our findings identified specific neural mechanisms at

play that should be considered in the clinical treatment of patients with optical defects. For instance, re-adaptation under improved optical correction devices could be combined with targeted perceptual learning paradigm[17] to enhance the speed, efficiency and generality of neural rehabilitation in patients with altered neural processing due to chronic exposure to poor optical quality.

In summary, our results are the first to assess the impact of long-term (years) exposure to severely degraded habitual optics on visual sensitivity to a wide range of SFs. Our findings support the presence of marked neural plasticity in the adult visual system, which allows the brain to longitudinally respond to optically-related sensory loss. Using AO correction, we were able to bypass optical factors and uncover a large-scale functional reorganization of neural sensitivity in KC participants mediated by SF-specific changes in signal enhancement mechanisms. The CSF can provide important insights into fundamental properties of human spatial vision, especially in individuals with spatial vision deficits[24,69]. The present study furthers our understanding of long-term neural adaptation mechanisms to various amounts of blur, showing that optical correction alone is unlikely to improve the patients' visual functioning. Instead, clinical rehabilitation approaches should take into consideration changes in neural sensitivity resulting from chronic exposure to poor optics. An important follow-up question in this context will be to assess how fast and to what extent the visual system of KC-afflicted individuals can re-adapt to a perfectly-corrected image.

Author contributions. A.B., K.R.H., D.T. and G.Y. designed the study. A.B. and G.Y. collected the data. A.B., W.J.P., R.Y.Z., D.T. and G.Y. analyzed the data. A.B., D.T. and G.Y. wrote the manuscript, and all authors commented on it.

Acknowledgements. This work was supported by NIH/NEI grant EY014999, the Research to Prevent Blindness, and the Schmitt Program on Integrative Neuroscience from the University of Rochester Medical Center. We thank Dr. Tara C. Vaz, O.D. and Dr. Len Zheleznyak for their help with participant screening and testing, as well as Olga Pikul for her help with patient recruitment.

Methods

Participants. A total of 9 keratoconus observers (KC1-9; mean age: 37±13, range: 24-55) and 9 neurotypical observers (NT1-9; mean age: 29±7, range: 21-45) participated in this study (see **Table S1** for demographic information). Participants were cyclopleged with tropicamide (1%) to dilate the pupil and paralyze accommodation during the experiment. All participants were screened prior to the study by one of our ophthalmologists, providing standard information (e.g., corneal curvature, refractive error) and ensuring that dilation was safe. An additional screening session was performed to ensure we could obtain good quality wavefront measurements and reach stable aberration-free condition under AO correction. Three potential KC participants did not pass this second screening stage and were not tested further along with KC1-9. The Research Subjects Review Board at the University of Rochester Medical Center approved all experimental protocols. Informed written consent was obtained from all participants prior to participation. Participants were compensated $12/hour.

Adaptive Optics Vision Simulator. An adaptive optics vision simulator (AOVS) allowed us to bypass any optical factors during psychophysical testing by measuring and correcting all monochromatic and polychromatic aberrations. As illustrated in a simplified schematic (**Fig.1b**; see also **Fig.S1**), the AOVS consisted of a custom-built Shack–Hartmann wavefront sensor to measure the wavefront aberrations, a deformable mirror (ALPAO DM97, Montbonnot, France) to correct subjects' wavefront aberrations, an artificial pupil set to 5.8 mm, and a calibrated visual display for psychophysical measurements. Wavefront aberrations were measured for a 6-mm pupil at fovea using an infrared (840±20 nm) superluminescent diode. The AOVS was operated in continuous closed loop (~8 Hz), allowing to fully correct all aberrations over a 6-mm pupil using with the deformable mirror. Visual testing was performed at fovea under white light conditions using a modified digital light processor display (Sharp XR-10X, Abeno-ku, Osaka, Japan) operating at 8 bits with 1024 X 768 (75 Hz) resolution, sustending 3.56º X 2.67º degrees of visual angle (dva). The display was calibrated with a PR-650 SpectraScan Colorimeter (Photo Research, Chatsworth, CA) and luminance precision was increased to 10.7 bits using the bitstealing technique. A dental impression bite bar mounted to motorized translation stages (x, y, z) with adjustable lateral headrests was used to stabilize head position and maintain pupil alignment during visual testing (**Fig.S1**).

Optical quality estimation. Wavefront measurements were collected for each observer using their everyday correction method, if any, allowing us to estimate each participant's habitual optical quality (**Fig.1c**). Wavefront aberrations were fitted to individual Zernike polynomials up to the 10th order, with 65 Zernikes coefficients. The square root of the sum of Zernikes coefficients aberrations was used to estimate the overall RMS error (total RMS: all Zernikes coefficients) and higher-order aberration (HOAs) RMS error (hRMS+: 6-65th Zernikes coefficients), reported in microns (μm). Wavefront measurements were also collected during visual testing to estimate both the quality and stability of the AO-correction (**Fig.1d**). Full correction of all Zernikes coefficients was applied for the entire duration of each testing session, with the exception of defocus for which appropriate defocus values were used to correct axial chromatic aberrations. Subjective defocus values were determined for all participants by asking them to adjust defocus using a motorized Badal prism to make a high-contrast Snellen letter "E" as sharp as possible, while correcting all other aberrations using AO. Then, through-focus high-contrast visual acuity measurements were used to objectively verify that the subjective defocus value applied during AO-correction resulted in a very focused, perceived image and maximal VA performance. After this initial session, each experimental session started with VA measurements to ensure the quality and stability of the AO correction before data collection. To maximize AO correction during stimulus presentation, participants were trained to blinks between trials and to stop if the perceptual quality got unstable or poor quality. To minimize the influence of blinks when estimating the residual RMS under AO correction,

the median RMS was computed across time for each measurement (**Fig.S2**). Then, the average residual RMS was computed for each participant from multiple wavefront measurements collected under AO correction (**Fig.1d**). As detailed and demonstrated in previous work[14-17,34], our AOVS provided stable, aberration-free optical quality during visual testing, in both typical and severely aberrated eyes.

Visual acuity measurements. Visual acuity (VA) thresholds were measured using a 4 alternative forced choice letter orientation task (**Fig.S4**), in which observers were judged whether a high-contrast Snellen "E" letter presented for 250 ms at fixation was oriented upward, downward, leftward or rightward. Stimuli were black letters presented on a white background. The size of each Snellen E letter was adjusted from trial-to-trial using the QUEST staircase method[70] to estimate 62.5%-correct VA thresholds (in logMAR), with 40 trials per staircase. Multiple VA thresholds were collected under AO correction for each participant. Each experimental session also started with VA testing to ensure the quality and stability of the AO correction before starting data collection.

Contrast sensitivity measurements. The contrast sensitivity function (CSF) of each participant was measured using a 2-AFC orientation discrimination task (**Fig.2a**). Each trial began with a dynamic fixation point. After a blank screen, a Gabor stimulus (Gaussian envelope SD: 0.75 dva; SF range: 0.25-30 cpd with 12 equal log-step values) oriented ±45° was presented at fovea. A 500-ms temporal Gaussian ramp was used to blend stimuli into the background and avoid onset/offset transients, and a brief tone signaled stimulus onset to reduce temporal uncertainty. Participants were asked to report whether the stimulus was tilted clockwise or counterclockwise. Auditory feedback was provided for both correct and incorrect responses. We used the *qCSF* method[24,35] to estimate 81%-correct contrast thresholds over a broad SF range. The *qCSF* method is a Bayesian adaptive strategy using *a priori* knowledge about the CSF's general form to obtain reasonably accurate estimates of sensitivity across SFs with as little as 50-100 trials. The *qCSF* method describes the CSF as a *truncated log-parabola* with four parameters (**Fig.2b**): (1) the peak sensitivity (amplitude) $CS_{\max}$; (2) the peak frequency SF_{peak}; (3) the bandwidth β (full width in octaves at half maximum); and (4) the truncation level at low SF δ. Without truncation, the CSF is defined as a function of the stimulus frequency (f) in decimal log as a *log-parabola CS´(f)*:

$$CS'(f) = \log_{10}(CS_{\max}) - \log_{10}(2)\left(\frac{\log_{10}(f) - \log_{10}(SF_{\text{peak}})}{\log_{10}(2\beta)/2}\right)^2 \qquad (1)$$

This *log-parabola* is then truncated at SF below the peak SF with the truncation parameter δ, which determines contrast sensitivity at low SF (CS_{low}):

$$CS(f) = CS'(f)\,, \qquad sf \geq SF_{\max}, \qquad (2)$$

$$CS_{\text{low}}(f) = \log_{10}(CS_{\max}) - \delta\,, \qquad sf < SF_{\max} \text{ and } SC'(f) < CS_{\max} - \delta$$

In addition, the high-SF cutoff (SF_{cutoff}) was estimated from the qCSF fits, corresponding to the frequency at which $CS(SF_{\text{cutoff}}) = 0$ (i.e., 100% contrast). The test procedure was similar to that described in previous studies[24,35]. Briefly, the stimulus space consisted of gratings with contrasts ranging from 0.1% to 99% in steps of 1.5 dB and SF from 0.25 to 30 cycles per degree (cpd). After familiarization with the task, participants performed around 6-7 qCSF runs of 100-trials each (mean number of runs: 6.8±2.6 for NTs, 7±2.8 for KCs), which were then combined to compute individual qCSF functions using all trials. Confidence intervals (95%-CIs) and p-values were computed from bootstrapping. Specifically, individual trials were randomly resampled with replacement to generate a resampled trial sequence,

which was refitted using the qCSF procedure. We repeated this procedure of resampling and refitting 10,000 times to generate bootstrap distributions of the fitted parameters. To assess statistical significance for differences in qCSF parameters and SF sensitivity estimates between groups, we derived difference distributions from bootstrap samples and determined p-values as the proportion of samples that "crossed" zero.

Equivalent noise paradigm. We used an equivalent noise paradigm[27-33] where perceptual thresholds are measured as a function of varying external noise levels added to the stimuli. Contrast thresholds were measured using a 2-AFC orientation discrimination task, for various amount of external noise (**Fig.4a**). Each trial began with a dynamic fixation point. After a blank screen, a ±45º oriented Gabor signal (cosine envelope diameter: 2 dva) embedded in different intensity levels of dynamic white noise (8 levels, from 0 to .33 SD) was presented at fovea for 100 ms. Participants were asked to report the orientation (±45º from the vertical) of the Gabor patch on each trial. Each stimulus was accompanied with a brief tone to reduce temporal uncertainty and auditory feedback was provided for both correct and incorrect responses. Stimulus presentation was controlled using the *FAST* method[40], an advanced adaptive psychophysical technique used to accurately estimate relevant model parameters in just 480 trials per participant for each SF. This allowed us to estimate contrast thresholds as a function of external noise contrast levels for both 70.71%- and 79.37%-correct difficulty levels, similar to previous studies[27-29,32,33]. Five different SFs (0.5, 1, 3, 9 and 16 cpd) were tested across different experimental sessions of 480 trials each (divided into 4 blocks of 120 trials). Data from the equivalent noise experiment were pooled from the *FAST* structures to estimate psychophysical thresholds for each participant at each of the external noise levels (60 trials per level). This approach yielded independent, albeit noisy, contrast threshold estimates at each noise level. Thresholds were estimated by fitting a Weibull function at each external noise level independently:

$$P(c) = 1 - (1 - 0.5) * 2^{-\left(\frac{\log(c)}{\alpha}\right)^{\eta}} \qquad (3)$$

where P denotes percent correct, c is stimulus contrast, α is contrast threshold at 75%-correct performance level, and η is the slope of the function. Similar to Park and colleagues[32], we used a Bayesian model fitting method implementing a Markov Chain Monte Carlo (MCMC) technique to estimate the two free parameters η and α. Specifically, we sampled the posterior distributions of the parameters using JAGS sofware (http://mcmc-jags.sourceforge.net). We assumed a broad uniform prior on each parameter with a range that includes all practically possible values. Maximum a posteriori (the mode of the posterior) were used as the best estimates of the model parameters. We discarded the first 15,000 samples as a burn-in period, and thinned the samples to reduce correlations by only selecting every 200 samples. A total of 10 chains were run in parallel, resulting in 1,000 posterior samples per chain. Thresholds at 70.71% and 79.37% were then computed from the estimated Weibull functions.

Conventional Perceptual Template Model (PTM) analysis. The PTM model[27-29] was used to estimate the sources of signal-to-noise changes responsible for performance differences between KC and typical observers. Contrast thresholds for two difficulty levels (70.71% and 79.37%) and across external noise levels were fitted with the PTM to quantify the effects of noise on contrast perception. The PTM consists of five main components (**Fig.4b**): a perceptual template tuned to the signal, a non-linear transducer function, a multiplicative internal noise source (N_{mul}), an additive internal noise source (N_{add}), and a decision process. The output of the perceptual template is processed by two pathways: the signal pathway in which the output is processed by an expansive nonlinear transducer function, and the multiplicative internal noise pathway in which the output is processed by a rectified nonlinear transducer function. Multiplicative noise is an independent noise source whose amplitude is

proportional to the (average) amplitude of the output from the perceptual template, acting as a contrast gain control mechanism. Additive internal noise is another noise source whose amplitude does not vary with signal strength, and is related to the gain of the perceptual template. Both multiplicative and additive noises are added to the output from template matching, and the noisy signal is submitted to a decision process. Here, contrast thresholds ($C_{\mathcal{T}}$) are characterized by:

$$C_{\mathcal{T}} = \frac{1}{\beta}\left[\frac{(1+N_{mul}^2)\,N_{ext}^{2\gamma} + N_{add}^2}{(1/d'^2 - N_{mul}^2)}\right]^{\frac{1}{2\gamma}} \qquad (4)$$

where the input (signal + external noise N_{ext}) is filtered through a perceptual template, resulting in signal enhancement via a gain factor β. The output of the filter is then transformed through a nonlinear transducer function that amplifies the inputs to the γth power, with both internal additive noise (N_{add}) and internal multiplicative noise (N_{mul}) being added to the output. N_{add} remains constant across signal levels, while N_{mul} is proportional to the signal strength. N_{ext} is manipulated by the experimenter along with the input signal. Finally, a decision process determines the contrast threshold at a specific performance level (d').

The PTM[27-29] considers that performance differences result from changes in three possible sources of inefficiency (**Fig.4b,c**): (1) changes in internal additive noise (A_{add}), reflecting signal enhancement of the perceptual template; (2) changes in external noise filtering (A_{ext}), corresponding to changes in signal selectivity (tuning) of the perceptual template; and (3) changes in internal multiplicative noise (A_{mul}), acting as a contrast gain control mechanism compressing the perceptual template's responses to signal contrast). Group averages of the independently estimated thresholds were used to fit the conventional PTM across SFs. To characterize group differences between NT and KC observers at each SF, the PTM introduces three coefficient indices (A_{mul}(SF,group), A_{add}(SF,group), and A_{ext}(SF,group)) to Equation (4):

$$C_{\mathcal{T}} = \frac{1}{\beta}\left[\frac{\left(1+\left(A_m(SF,group)*N_{mul}(SF)\right)^2\right)\left(A_e(SF,group)*N_{ext}\right)^{2\gamma}+\left(A_a(SF,group)*N_{add}(SF)\right)^2}{\left(\frac{1}{d'^2}-\left(A_m(SF,group)*N_{mul}(SF)\right)^2\right)}\right]^{\frac{1}{2\gamma}} \qquad (5)$$

The coefficient indices for NT are fixed to 1 (A_{mul}(NT) = A_{add}(NT) = A_{ext}(NT) = 1). N_{add}(SF) and N_{mul}(SF) did not vary across groups, only across SFs to reflect differences in contrast thresholds related to stimulus SF. To estimate whether and how these three types of noise could account for group differences in KC group(s), we computed the relative differences in the effects of each source of noise between the groups. Elevated sources of noise in KC relative to NT would correspond to A_{mul}(KC), A_{add}(KC), and/or A_{ext}(KC) estimates being higher than 1 (i.e., NT group), and to poorer contrast thresholds. Conversely, reduced sources of noise in KC relative to NT would correspond to estimates lower than 1, and to better contrast thresholds. These three coefficient indices for each KC group could be restricted, either varying or fixed at 1. We compared the results obtained by fitting the eight possible models (**Fig.S5-8** and **Table S2**), ranging from no change in any of the three noise-reduction mechanisms in KC groups to the full model with changes in all three noise-reduction mechanisms. We compared the NT group to 2 groups of KC participants (mild/moderate and severe) at 5 different SFs. The full model consisted of 12 shared parameters across groups (β, γ, N_{mul}(SF1-5), N_{add}(SF1-5)), and fifteen noise parameters (A_{mul}(SF1-5) = A_{add}(SF1-5) = A_{ext}(SF1-5)) for each of the two KC groups, for a total of 42 parameters. Model fitting was carried out using a least-square method, and goodness-of-fit (r^2) for each candidate model was computed as follows:

$$r^2 = 1 - \frac{\sum \left[\log\left(C_{\mathcal{T}}^{predicted}\right) - \log\left(C_{\mathcal{T}}\right)\right]^2}{\sum \left[\log(C_{\mathcal{T}}) - mean(\log(C_{\mathcal{T}}))\right]^2} \quad (6)$$

where $\sum$ and $mean$ were computed across groups, SFs, external noise levels, and difficulty levels. Given the large differences in the number of free parameters across models, we computed the Bayesian Information Criterion (BIC) as criterion for model selection. The BIC selects the best model while correcting for overfitting by introducing a penalty term for the number of free parameters in the model:

$$BIC = n * \log\left(\frac{RSS}{n}\right) + k * \log(n) \quad (7)$$

where n being the number of predicted data points, RSS is the residual sum of squares of the model, and k is the number of parameters of the model. BIC approximates a transformation of a model's posterior probability. We then computed ΔBIC as:

$$\Delta BIC^k = BIC^k - BIC^{k^*} \quad (8)$$

where k^* correspond to the model with the lowest BIC value (i.e., the best model).

Hierarchical Bayesian PTM analysis. To better assess for links between habitual optical quality and individual variability in the PTM noise estimates, we used a hierarchical Bayesian modeling technique to fit the PTM to each participant. This technique assumes that each participant is drawn from a population distribution (NT or KC), which increases statistical power. Importantly, this technique allows estimation of PTM parameters for each participant within a population, providing a better understanding of individual variability. We assumed that individual's response for a given trial is drawn from a Bernoulli distribution (i.e., $response_{ijk} \sim Bernoulli(\theta_{ijk})$), where i is the difficulty level, j is the external noise level (N_{ext}), and k is the trial number. θ_{ijk} corresponds to the probability of making a correct response:

$$\theta_{ijk} = 1 - (1 - 0.5) * e^{\left(\frac{m_i \log(x_{ijk})}{\log(C_{\tau ij})}\right)^{\eta}} \quad (9)$$

where x corresponds to the stimulus contrast, η to the slope, $C_{\tau ij}$ to the contrast threshold, and m_i to:

$$m_i = -\log\left(\frac{1-q_i}{1-0.5}\right)^{\frac{1}{\eta}} \quad (10)$$

The parameter q_i corresponds to the difficulty level (i.e., either .7071 or .7937). The PTM defined the contrast threshold $C_{\tau ij}$ as:

$$C_{\tau ij} = \frac{1}{\beta}\left[\frac{\left(1+N_{mul}^2\right)\left(w_{ext}\, N_{ext_{ij}}\right)^{2\gamma} + N_{add}^2}{\left(1/d'^2_i - N_{mul}^2\right)}\right]^{\frac{1}{2\gamma}} \quad (11)$$

Equation (11) is the same as Equation (4), except for the fact that a coefficient for external noise (w_{ext}) is added here to characterize the impact of external noise on individual's contrast thresholds. For each participant, we estimated three parameters N_{mul}, N_{add}, and w_{ext}. We assumed a fixed β (1.25) and γ (2) for all participants to simplify the model, which was within a reasonable range reported in previous

656 studies[27-29,32]. Similar to the Weibull fitting procedure, an MCMC technique was used to sample from the
657 posterior distributions and estimate the free parameters. Here, we assumed hierarchical priors on each
658 of the model parameters, meaning that each model parameter that characterized an individual
659 participant was assumed to be drawn from an independent Gaussian population distribution with a
660 mean and SD that characterized each group (NT or KC). Priors for population means and SDs were set to
661 broad uniform distributions. Maximum a posteriori were used as the best parameter estimates for both
662 individual and population parameters. We used 15,000 iterations for burn-in, and only selected every
663 200 samples for thinning. Ten chains were run in parallel, each of which sampled 2,000 posterior
664 samples.

665 **References**

666 1 Artal, P. Aging Effects on the Optics of the Eye. *In: Cavallotti, C.A.P., Cerulli, L. (eds). Age-Related Changes of*
667 *the Human Eye. Aging Medicine. Humana Press.* (2008).

668 2 Webster, M. A. Adaptation and visual coding. *J Vis* **11** (2011).

669 3 Webster, M. A. Visual Adaptation. *Annu Rev Vis Sci* **1**, 547-567 (2015).

670 4 George, S. & Rosenfield, M. Blur adaptation and myopia. *Optom Vis Sci* **81**, 543-547 (2004).

671 5 Mon-Williams, M., Tresilian, J. R., Strang, N. C., Kochhar, P. & Wann, J. P. Improving vision: neural
672 compensation for optical defocus. *Proc Biol Sci* **265**, 71-77 (1998).

673 6 Webster, M. A., Georgeson, M. A. & Webster, S. M. Neural adjustments to image blur. *Nat Neurosci* **5**, 839-840
674 (2002).

675 7 Artal, P. *et al.* Neural compensation for the eye's optical aberrations. *J Vis* **4**, 281-287 (2004).

676 8 Bao, M. & Engel, S. A. Distinct mechanism for long-term contrast adaptation. *Proc Natl Acad Sci U S A* **109**,
677 5898-5903 (2012).

678 9 Bao, M., Fast, E., Mesik, J. & Engel, S. Distinct mechanisms control contrast adaptation over different
679 timescales. *J Vis* **13** (2013).

680 10 Glasser, D. M., Tsui, J. M., Pack, C. C. & Tadin, D. Perceptual and neural consequences of rapid motion
681 adaptation. *Proc Natl Acad Sci U S A* **108**, E1080-1088 (2011).

682 11 Marcos, S. *et al.* Vision science and adaptive optics, the state of the field. *Vision Res* **132**, 3-33 (2017).

683 12 Yoon, G. Y. & Williams, D. R. Visual performance after correcting the monochromatic and chromatic
684 aberrations of the eye. *J Opt Soc Am A Opt Image Sci Vis* **19**, 266-275 (2002).

685 13 Liang, J., Williams, D. R. & Miller, D. T. Supernormal vision and high-resolution retinal imaging through
686 adaptive optics. *J Opt Soc Am A Opt Image Sci Vis* **14**, 2884-2892 (1997).

687 14 Zheleznyak, L., Barbot, A., Ghosh, A. & Yoon, G. Optical and neural anisotropy in peripheral vision. *J Vis* **16**, 1
688 (2016).

689 15 Sabesan, R., Ahmad, K. & Yoon, G. Correcting highly aberrated eyes using large-stroke adaptive optics. *J*
690 *Refract Surg* **23**, 947-952 (2007).

691 16 Sabesan, R. & Yoon, G. Visual performance after correcting higher order aberrations in keratoconic eyes. *J Vis*
692 **9**, 6 1-10 (2009).

693 17 Sabesan, R., Barbot, A. & Yoon, G. Enhanced neural function in highly aberrated eyes following perceptual
694 learning with adaptive optics. *Vision Res* (2016).

695 18 Maeda, N. *et al.* Wavefront aberrations measured with Hartmann-Shack sensor in patients with keratoconus.
696 *Ophthalmology* **109**, 1996-2003 (2002).

19 Pantanelli, S., MacRae, S., Jeong, T. M. & Yoon, G. Characterizing the wave aberration in eyes with keratoconus or penetrating keratoplasty using a high-dynamic range wavefront sensor. *Ophthalmology* **114**, 2013-2021 (2007).

20 DeValois, R. L. & DeValois, K. K. *Spatial Vision*. (New York: Oxford University Press., 1988).

21 Campbell, F. W. & Green, D. G. Optical and retinal factors affecting visual resolution. *J Physiol* **181**, 576-593 (1965).

22 Blakemore, C. & Campbell, F. W. On the existence of neurones in the human visual system selectively sensitive to the orientation and size of retinal images. *J Physiol* **203**, 237-260 (1969).

23 Fechner, G. T. *Elemente der Psychophysik. Leipzig: Breithopf und Hertel, 1860*. (In: Elements of Psychophysics, edited by Howes DH and Boring EC; translated by Adler HE. New York: Holt, Rinehart, and Winston, 1966., 1860).

24 Hou, F. *et al.* qCSF in clinical application: efficient characterization and classification of contrast sensitivity functions in amblyopia. *Invest Ophthalmol Vis Sci* **51**, 5365-5377 (2010).

25 Guy, J., Mottron, L., Berthiaume, C. & Bertone, A. The developmental trajectory of contrast sensitivity in autism spectrum disorder. *Autism Res* **9**, 866-878 (2016).

26 Yan, F. F., Hou, F., Lu, Z. L., Hu, X. & Huang, C. B. Efficient Characterization and Classification of Contrast Sensitivity Functions in Aging. *Sci Rep* **7**, 5045 (2017).

27 Dosher, B. A. & Lu, Z. L. Perceptual learning reflects external noise filtering and internal noise reduction through channel reweighting. *Proc Natl Acad Sci U S A* **95**, 13988-13993 (1998).

28 Dosher, B. A. & Lu, Z. L. Mechanisms of perceptual learning. *Vision Res* **39**, 3197-3221 (1999).

29 Lu, Z. L. & Dosher, B. A. Characterizing observers using external noise and observer models: assessing internal representations with external noise. *Psychol Rev* **115**, 44-82 (2008).

30 Burgess, A. E., Wagner, R. F., Jennings, R. J. & Barlow, H. B. Efficiency of human visual signal discrimination. *Science* **214**, 93-94 (1981).

31 Pelli, D. G. & Farell, B. Why use noise? *J Opt Soc Am A Opt Image Sci Vis* **16**, 647-653 (1999).

32 Park, W. J., Schauder, K. B., Zhang, R., Bennetto, L. & Tadin, D. High internal noise and poor external noise filtering characterize perception in autism spectrum disorder. *Sci Rep* **7**, 17584 (2017).

33 Bejjanki, V. R. *et al.* Action video game play facilitates the development of better perceptual templates. *Proc Natl Acad Sci U S A* **111**, 16961-16966 (2014).

34 Sabesan, R., Zheleznyak, L. & Yoon, G. Binocular visual performance and summation after correcting higher order aberrations. *Biomed Opt Express* **3**, 3176-3189 (2012).

35 Lesmes, L. A., Lu, Z. L., Baek, J. & Albright, T. D. Bayesian adaptive estimation of the contrast sensitivity function: the quick CSF method. *J Vis* **10**, 17 11-21 (2010).

36 Thurman, S. M., Davey, P. G., McCray, K. L., Paronian, V. & Seitz, A. R. Predicting individual contrast sensitivity functions from acuity and letter contrast sensitivity measurements. *J Vis* **16**, 15 (2016).

37 Dorr, M. *et al.* Evaluation of the precision of contrast sensitivity function assessment on a tablet device. *Sci Rep* **7**, 46706 (2017).

38 Jia, W. *et al.* The effects of monocular training on binocular functions in anisometropic amblyopia. *Vision Res* **152**, 74-83 (2018).

39 Hou, F. *et al.* Evaluating the performance of the quick CSF method in detecting contrast sensitivity function changes. *J Vis* **16**, 18 (2016).

40 Vul, E., Bergsma, J. & MacLeod, D. I. Functional adaptive sequential testing. *Seeing Perceiving* **23**, 483-515

739 (2010).

740 41 Lu, Z. L. & Dosher, B. A. External noise distinguishes attention mechanisms. *Vision Res* **38**, 1183-1198 (1998).

741 42 Lu, Z. L. & Dosher, B. A. Spatial attention excludes external noise without changing the spatial frequency
742 tuning of the perceptual template. *J. Vis.* **4**, 955-966 (2004).

743 43 Dosher, B. A. & Lu, Z. L. Noise exclusion in spatial attention. *Psychol Sci* **11**, 139-146 (2000).

744 44 Levi, D. M. & Klein, S. A. Noise provides some new signals about the spatial vision of amblyopes. *J Neurosci* **23**,
745 2522-2526 (2003).

746 45 Sperling, A. J., Lu, Z. L., Manis, F. R. & Seidenberg, M. S. Deficits in perceptual noise exclusion in developmental
747 dyslexia. *Nat Neurosci* **8**, 862-863 (2005).

748 46 Cavanaugh, M. R. *et al.* Visual recovery in cortical blindness is limited by high internal noise. *J Vis* **15**, 9 (2015).

749 47 Banks, M. S., Geisler, W. S. & Bennett, P. J. The physical limits of grating visibility. *Vision Res* **27**, 1915-1924
750 (1987).

751 48 Osborne, L. C., Lisberger, S. G. & Bialek, W. A sensory source for motor variation. *Nature* **437**, 412-416 (2005).

752 49 Rajeev, N. & Metha, A. Enhanced contrast sensitivity confirms active compensation in blur adaptation. *Invest*
753 *Ophthalmol Vis Sci* **51**, 1242-1246 (2010).

754 50 Webster, M. A. Contrast sensitivity under natural states of adaptation. *Proc. SPIE 3644, Human Vision and*
755 *Electronic Imaging IV* (1999).

756 51 Ghodrati, M., Zavitz, E., Rosa, M. G. P. & Price, N. S. C. Contrast and luminance adaptation alter neuronal
757 coding and perception of stimulus orientation. *Nat Commun* **10**, 941 (2019).

758 52 Gepshtein, S., Lesmes, L. A. & Albright, T. D. Sensory adaptation as optimal resource allocation. *Proc Natl Acad*
759 *Sci U S A* **110**, 4368-4373 (2013).

760 53 Sharpee, T. O. *et al.* Adaptive filtering enhances information transmission in visual cortex. *Nature* **439**, 936-942
761 (2006).

762 54 Gutnisky, D. A. & Dragoi, V. Adaptive coding of visual information in neural populations. *Nature* **452**, 220-224
763 (2008).

764 55 Sabesan, R. & Yoon, G. Neural compensation for long-term asymmetric optical blur to improve visual
765 performance in keratoconic eyes. *Invest Ophthalmol Vis Sci* **51**, 3835-3839 (2010).

766 56 Boynton, G. M., Demb, J. B., Glover, G. H. & Heeger, D. J. Neuronal basis of contrast discrimination. *Vision Res*
767 **39**, 257-269 (1999).

768 57 Meng, J. *et al.* Neural correlates of stimulus spatial frequency-dependent contrast detection. *Exp Brain Res*
769 **225**, 377-385 (2013).

770 58 Niemeyer, J. E. & Paradiso, M. A. Contrast sensitivity, V1 neural activity, and natural vision. *J Neurophysiol* **117**,
771 492-508 (2017).

772 59 Kelly, D. H. Spatial frequency selectivity in the retina. *Vision Res* **15**, 665-672 (1975).

773 60 Carandini, M. & Heeger, D. J. Normalization as a canonical neural computation. *Nat Rev Neurosci* **13**, 51-62
774 (2012).

775 61 Fournier, J., Monier, C., Pananceau, M. & Fregnac, Y. Adaptation of the simple or complex nature of V1
776 receptive fields to visual statistics. *Nat Neurosci* **14**, 1053-1060 (2011).

777 62 Bauman, L. A. & Bonds, A. B. Inhibitory refinement of spatial frequency selectivity in single cells of the cat
778 striate cortex. *Vision Res* **31**, 933-944 (1991).

779 63 De Valois, K. K. & Tootell, R. B. Spatial-frequency-specific inhibition in cat striate cortex cells. *J Physiol* **336**,

780 359-376 (1983).

781 64 Bredfeldt, C. E. & Ringach, D. L. Dynamics of spatial frequency tuning in macaque V1. *J Neurosci* **22**, 1976-1984
782 (2002).

783 65 Kohn, A. Visual adaptation: physiology, mechanisms, and functional benefits. *J Neurophysiol* **97**, 3155-3164
784 (2007).

785 66 Kumano, H. & Uka, T. Neuronal mechanisms of visual perceptual learning. *Behav Brain Res* **249**, 75-80 (2013).

786 67 Lu, Z. L., Hua, T., Huang, C. B., Zhou, Y. & Dosher, B. A. Visual perceptual learning. *Neurobiol Learn Mem* **95**,
787 145-151 (2011).

788 68 McGovern, D. P., Roach, N. W. & Webb, B. S. Perceptual learning reconfigures the effects of visual adaptation.
789 *J Neurosci* **32**, 13621-13629 (2012).

790 69 Ginsburg, A. P. Contrast sensitivity and functional vision. *Int Ophthalmol Clin* **43**, 5-15 (2003).

791 70 Watson, A. B. & Pelli, D. G. QUEST: a Bayesian adaptive psychometric method. *Percept Psychophys* **33**, 113-120
792 (1983).